IEEE Access
Multidisciplinary | Rapid Review | Open Access Journal

Received March 26, 2019, accepted March 29, 2019, date of publication April 2, 2019, date of current version April 17, 2019.

*Digital Object Identifier 10.1109/ACCESS.2019.2908885*

# Detection of a Conductive Object Embedded in an Optically Opaque Dielectric Medium by the Thermo-Elastic Optical Indicator Microscopy

**HANJU LEE[1], ZHIRAYR BAGHDASARYAN[1], BARRY FRIEDMAN[2], AND KIEJIN LEE[1]**
[1]Department of Physics and Basic Science Institute for Cell Damage Control, Sogang University, Seoul 121-742, South Korea
[2]Department of Physics, Sam Houston State University, Huntsville, TX 77341, USA

Corresponding author: Kiejin Lee (klee@sogang.ac.kr)

This work was supported in part by the Basic Science Research Program through the National Research Foundation of Korea (NRF) funded by the Ministry of Education under Grant NRF-2018R1D1A1B07047984, in part by the Basic Science Research Program through the National Research Foundation of Korea under Grant 2015R1D1A1A02061824 and Grant 2009-0093822, and in part by the International Cooperation Program managed by the National Research Foundation of Korea under Grant NRF-2018K2A9A1A01090496.

**ABSTRACT** We present a new method for the subsurface imaging of a conductive object embedded in a dielectric medium based on microwave imaging by thermo-elastic optical indicator microscopy. The present method is based on the imaging of the microwave near field distribution generated by a conductive object embedded in a dielectric medium. When the thickness of the dielectric medium is small so that the microwave near field generated by the conductive object can emerge from the dielectric medium, one can find the presence of the object by visualizing the microwave distribution appearing on the surface of the medium. By using the present method, we visualized the microwave field distribution appearing on a surface of a dielectric medium containing a conductive object with an irradiating microwave. We observed that strong microwave near fields that were present around the conductive object appeared on the surface of the dielectric medium, and their intensities were dependent on the frequency and polarization direction of the irradiated microwave. By visualizing various conductive lines having different lengths of 4∼10 mm with a width of 1 mm, and buried depths of 1∼5 mm, we showed that the present method can be a practical nondestructive and noncontact way for the detection of conductive lines and structures embedded in an optically opaque dielectric medium.

**INDEX TERMS** Microwave imaging, subsurface imaging, optical inspection technology.

## I. INTRODUCTION

Non-destructive detection of buried or hidden objects by means of microwave imaging has various applications [1]. Its applications include subsurface imaging of an electrical circuit embedded in a dielectric film [2], imaging of a buried dopant nanostructure in a semiconductor [3], [4], defect detection located in the volume of a metal sample [5], non-invasive detection of breast cancer [6], detection of damage within a concrete structure [7]. This diversity comes from the fact that the microwaves penetrate well into dielectric materials, and thin films of semiconductors and metals.

Existing methods for the subsurface microwave imaging are usually based on an electrical measurement by using scanning probe methods and antennas [1]–[7]. The scanning probe methods have advantages in that the spatial resolution can reach the nanoscale range [3], [4]. However, a slow measurement throughput caused by the spatial scanning of the probe limits their practical applications. While modern antenna methods such as the multispectral time-of-flight microwave imaging [8], and microwave imaging methods based on metamaterials [9], [10] can provide outstanding measurement throughput, their spatial resolutions are limited by the wavelength of the microwave and the size of the resonant element composing the metamaterial structure.

Optical microscopy using a parallelized sensor arrays such as the charged coupled device (CCD) camera will be a

The associate editor coordinating the review of this manuscript and approving it for publication was Chao Zuo.

candidate that can overcome the limitations of the conventional scanning and the antenna method. Indeed, optical techniques based on the electro-optical effect with a modified complementary metal-oxide-semiconductor (CMOS) sensor array showed an outstanding performance in the measurement throughput and the spatial resolution [11], [12]. However, these methods have a disadvantage in practical applications because they require special and expensive materials and devices.

Previously, we reported a new optical method, thermo-elastic optical indicator microscopy (TEOIM) [13]. The TEOIM is composed of a conventional polarized light microscope and an optical indicator (OI). The OI of the TEOIM is composed of a typical slide glass coated by a thin film that is heated by the microwave. It converts the microwave signal to an optical signal through the photo-elastic effect induced by a thermal stress in the glass substrate that is caused by microwave heating of the coated thin film. While the TEOIM uses conventional materials and devices, it can provide optical resolution with a wide field of view, a broad microwave frequency bandwidth, selectivity for microwave electric and magnetic field imaging, and real time measurement throughput.

In this paper, we present a practical application of the TEOIM for the subsurface detection of a conductive object embedded in an optically opaque dielectric medium. By using a slide glass coated by indium tin oxide (ITO) as the OI of the TEOIM, we visualized the microwave magnetic field distribution appearing on the surface of the dielectric material containing a conductive object. We tested various sizes of conductive objects with different microwave frequencies, and polarization direction of the excitation microwave field to investigate the inspection performance for the subsurface detection of the conductive object. From the measurement results, we showed that one can find the embedded conductive object from the microwave magnetic field distribution appearing on the surface of the dielectric material.

## II. MEASUREMENT PRINCIPLE

Figure 1 (a) illustrates the measurement principle of the TEOIM for the subsurface detection of the conductive object embedded in an optically opaque dielectric medium. Here we assume that the dielectric loss of the medium is small so that the microwave signal can be transmitted through the medium. When a microwave is radiated to such a low loss medium containing a conductive object, the microwave will penetrate well into the medium so that it will interact with the embedded object. This interaction will create the microwave near field around the conductive object, and the structure of the near field will depend on the shape of the conductive object, frequency and polarization of the irradiated microwave signal. For instance, if the conductive object can be assumed to be a line with a narrow width, it will behave as an open ended strip-line resonator so that a strong near field will appear at a particular microwave frequency and polarization direction satisfying the resonance condition. In this case, if the thickness of the dielectric medium is thin enough compared to the near field region of the conductive object, one can detect the object by measuring the microwave near field emerging from the dielectric medium.

The microwave near field structure can be visualized by placing the OI of the TEOIM in the near field region. The OI of the TEOIM is composed of a glass substrate coated by a thin film that is well heated by the microwave. When the OI is placed in the microwave near field region, the thin film will be heated by the microwave electric or magnetic field depending on its loss property. For instance, it is known that a conductive thin film is heated by the microwave magnetic field by the inductive heating process [14], [15]. Therefore, if the OI is made of a glass substrate coated by a conductive thin film, it will be heated depending on the spatial distribution of the magnetic microwave near field (H-MWNF). In this case, one can visualize the H-MWNF distribution by visualizing the heat source distribution of the OI [13].

The heat source distribution of the OI can be visualized by analyzing the thermal stress distribution that can obtained from the photo-elastic effect of the glass substrate. When the thin film is heated by microwave, the generated heat is diffused into the glass substrate. This results in a thermal stress of the glass substrate of the OI, and the stress distribution is dependent on the heating distribution of the coated thin film. When a circularly polarized light propagates through such a stressed glass substrate, the circularly polarized state is changed into an elliptically polarized state depending on the local stress state by the photo-elastic effect. Then, by analyzing the distribution of the elliptically polarized state of the reflected light, one can obtain the heat source density distribution causing the thermal stress, which is identical to the microwave near field distribution, through the plane thermal stress analysis [11], [16].

## III. EXPERIMENT

### A. MEASUREMENT SETUP

Figure 1(b) illustrates the measurement setup. We used commercially available ITO coated glass substrate as the OI. Because the ITO thin film has a high electrical conductivity, it is well heated by the microwave magnetic field through the inductive heating process [14], [15]. Therefore, the measured heat source distribution corresponds to the H-MWNF distribution emitted from the object. The ITO thin film (thickness: 50 nm) was coated on a soda lime glass substrate (60 mm by 60 mm by 0.5 mm) by the sputtering method. The ITO coated glass was placed on the sample with an air gap of 1 mm, where the air gap was introduced to reduce the direct heat conduction from the sample. The ITO surface was faced to the sample while the glass substrate was faced to the optical measurement system. In this configuration, the probing light propagated through the glass substrate, and it was reflected at the interface of ITO and glass substrate.

The polarization state of the incident light emitted from a light emitting diode (LED, $\lambda = 530$ nm) was modulated to be left-handed and right-handed circularly

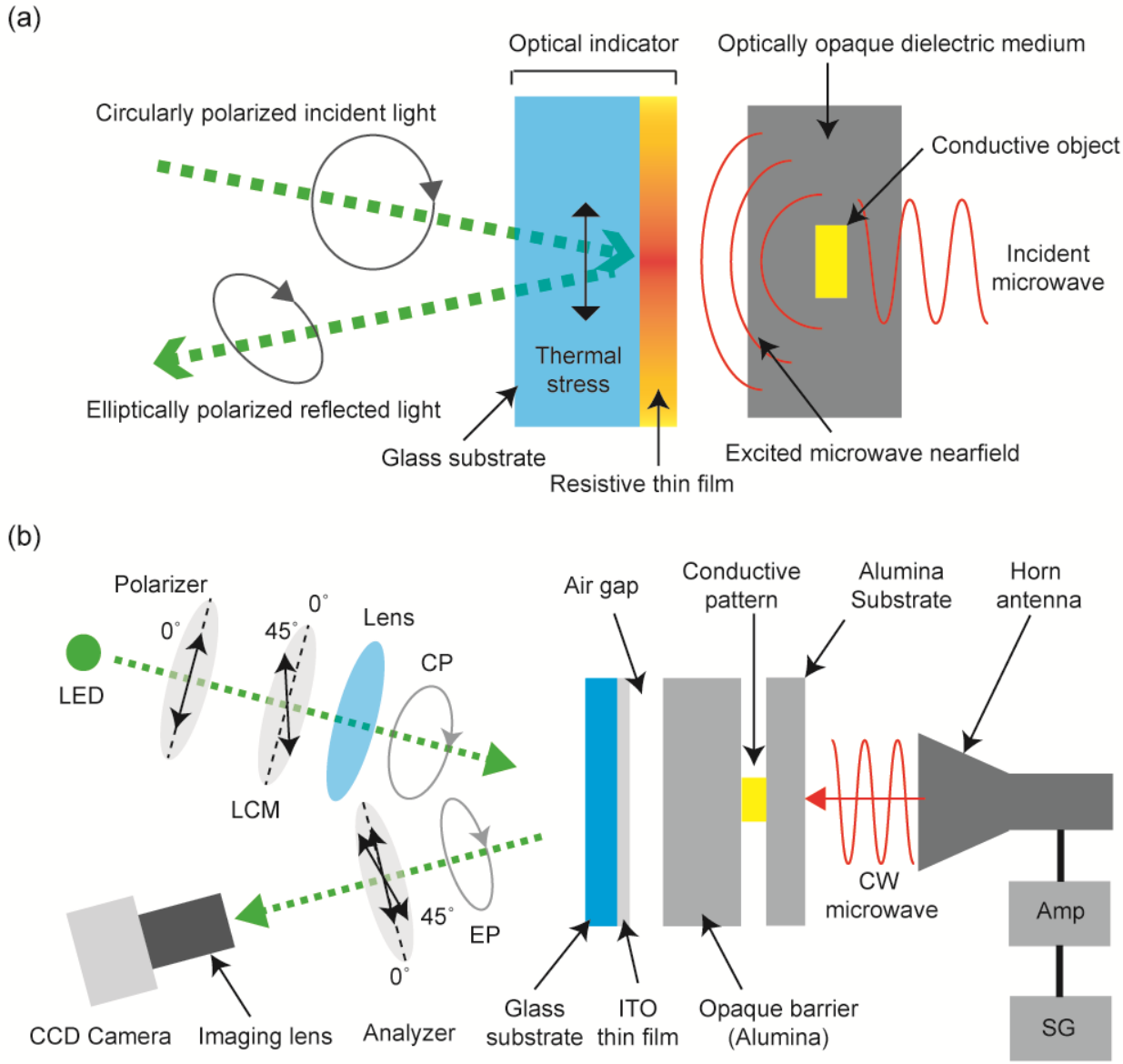


**FIGURE 1.** Illustration of measurement principle. The microwave (MW) signal propagates to a dielectric medium containing a conductive object. Microwave near field of the conductive object excited by the propagating microwave signal emerge out from the dielectric medium, and it interacts with an optical indicator (OI) that is composed of glass substrate coated by a resistive thin film. The generated heat by the microwave heating of the resistive thin film is transferred to the glass substrate. A thermal stress appears in the glass substrate by the transferred heat, and it results in the photo-elastic effect. By the photo-elastic effect induced by thermal stress, a circularly polarized light propagating in the glass substrate is changed to an elliptically polarized light. (b) Illustration of measurement setup. The light emitting diode (LED, $\lambda = 530$nm) was used for the light source. The dashed green lines indicate the propagation path of probing light. The polarization state of the probing light is modulated to be circularly polarized (CP) states by using a linear polarizer and a liquid crystal modulator (LCM). The polarization state of the reflected light from the indicator is changed to an elliptically polarized (EP) state by the photo-elastic effect of the indicator, and the change is measured by using an analyzer (sheet polarizer) and charge coupled device (CCD) camera. Orientations of optical axes of the polarizer, LCM, and analyzer are indicated by bidirectional arrows (black). The microwave (MW) signal generated by a signal generator (SG) is amplified by an amplifier and is transmitted to the horn antenna. The emitted MW from the horn antenna propagates to the sample. The sample is fabricated by attaching an alumina substrate having a conductive pattern to a thick alumina plate.

polarized (LCP and RCP) states by using a linear polarizer and a liquid crystal modulator (LCM). The LCM is an electrically tunable linear retarder so that one can obtain circularly polarized states by applying a proper electrical voltage to the LCM [13], [17]. We aligned optical axes of the polarizer and LCM to make 45° to maximize the range of the polarization modulation. The reflected light from the optical indicator propagated to the analyzer (sheet polarizer), and the light intensity transmitted from the analyzer was measured by a charge coupled device (CCD) camera.

A microwave signal generator (SG) was used as the microwave source. The generated (power: 0 dBm) signal was transferred to a high power amplifier (Amp) through a coaxial cable. For the experiment, we used continuous wave signal (CW). The microwave frequency was controlled by a custom program using the GPIB communication. The power

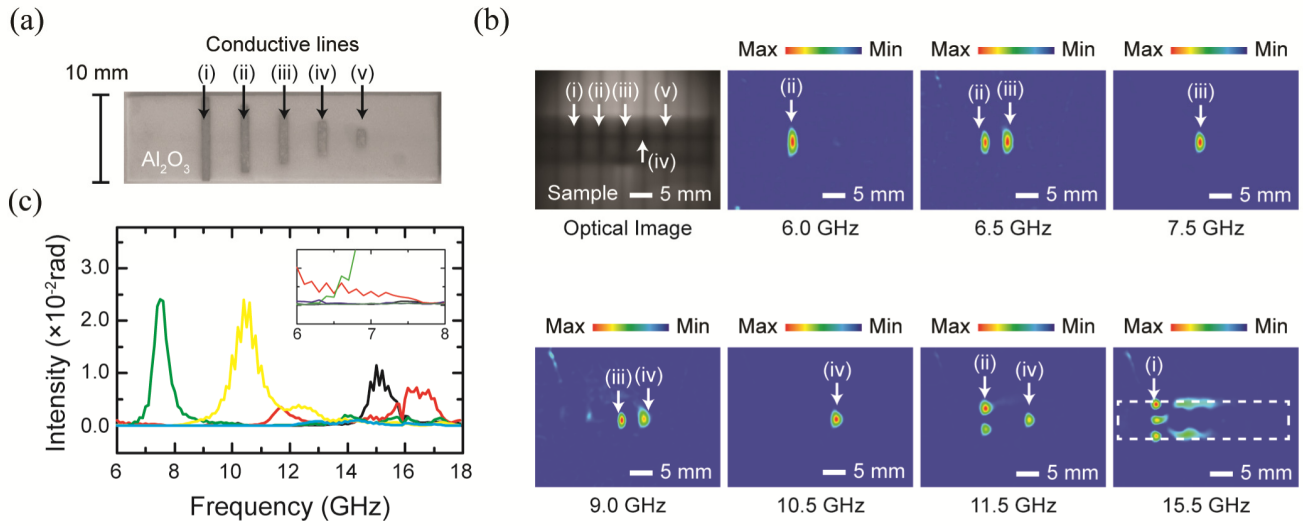


**FIGURE 2.** Optical image of the sample used in the experiment. Conductive lines having different lengths with same width (1 mm) are indicated by arrows: (i) 10 mm; (ii) 8 mm; (iii) 6 mm; (iv) 4 mm; (v) 2 mm. (b) Representative images of the magnetic microwave near field distributions of conductive lines measured by the TEOIM for different input microwave frequency with a field of view of 40 mm (width) by 30mm (height). We normalized each image with respect to its mazimum intensity to show the structure of the magnetic microwave near field distribution because the intensity was dependent on the microwave frequency. We indicated white solid lines in images corresponding to 5mm length. The optical image shows the sample covered by a alumina substrate. This optical image was obtained by illuminating a light to the sample covered by an alumina from its backside. We note that the sample was optically invisible when the backside illumination of the light was stopped. (c) Local intensity changes of measured magnetic microwave near field by the TEOIM around conductive lines (i-v) as a function of input microwave frequency: (i) black; (ii) red; (iii) green; (iv) yellow; (v) cyan.

of the amplified microwave signal was 30 dBm, and the amplified microwave signal was transferred to a horn antenna through a coaxial cable. The horn antenna was placed behind the sample with a distance of 1 cm. This distance was introduced to change the sample without changing the position of the optical indicator.

We used an alumina plate for the optically opaque dielectric material, where width, height, and thickness of the plate were 60 mm, 60mm, and 1mm, respectively. For the fabrication of conductive objects, we used silver sintering paste. We first coated the silver paste on an alumina substrate, and then, we fabricated patterns of conductive objects by removing the silver paste through the laser patterning method. Finally, the patterned alumina substrate was sintered for 1 hour at 900°C to remove the resin of the silver paste. After fabrication of the conductive pattern, we attached a bare alumina substrate on the patterned alumina substrate so that the conductive patterns were optically invisible. To fabricate samples having different thickness of the opaque barrier, we attached 1∼4 bare alumina substrates (thickness: 1mm) on the conductive patterns.

### B. IMAGING PROCESS

Two images, $\beta_1$ and $\beta_2$ that were related to the normal and shear stress distributions of the OI [13], were calculated from measured images with different polarization states of the probing light and the orientations of the optical axis of the analyzer by the following equation [13], [16]:

$$\beta_1(x,y) = \frac{1}{2}\frac{I_{\mathrm{LCP},\pi/4}(x,y) - I_{\mathrm{RCP},\pi/4}(x,y)}{I_{\mathrm{LCP},\pi/4}(x,y) + I_{\mathrm{RCP},\pi/4}(x,y)}, \quad (1)$$

$$\beta_2(x,y) = \frac{1}{2}\frac{I_{\mathrm{LCP},\pi/2}(x,y) - I_{\mathrm{RCP},\pi/2}(x,y)}{I_{\mathrm{LCP},\pi/2}(x,y) + I_{\mathrm{RCP},\pi/2}(x,y)}, \quad (2)$$

where, $I$ is the measured intensity distribution by the CCD camera, LCP and RCP are the polarization states of reflected light from the OI, $\pi/2$, $\pi/4$ are angles of the optical axis of the analyzer to that of polarizer. Intensity measurements were conducted 1000 times for each polarization state and analyzer angle with and without microwave irradiation, and each measured image was averaged. The measured images with microwave irradiation were subtracted by images measured without microwave irradiation to remove background intensity signals caused by stray light.

The heat source distribution was calculated from $\beta_1$ and $\beta_2$ by the following equation [13], [16]:

$$\frac{q(x,y)}{C} = 2\frac{\partial^2\beta_2(x,y)}{\partial x\partial y} + \frac{\partial^2\beta_1(x,y)}{\partial x^2} - \frac{\partial^2\beta_2(x,y)}{\partial y^2}, \quad (3)$$

where $C$ is a constant related to the wavelength of the light, thickness and stress optical constant of the glass substrate. In the practical calculation for equation (3), we calculated the differentiation of the $\beta_1$ and $\beta_2$ by calculating the intensity difference between the adjacent pixels. In addition, we smoothed the images by taking a moving average before the differentiations. One can find further details on the measurement and calculation processes in our previous papers [13], [16].

## IV. RESULT AND DISCUSSION

Figure 2(a-b) shows optical image of the sample used in experiments, and representative H-MWNF distributions measured by TEOIM. To investigate the performance of the

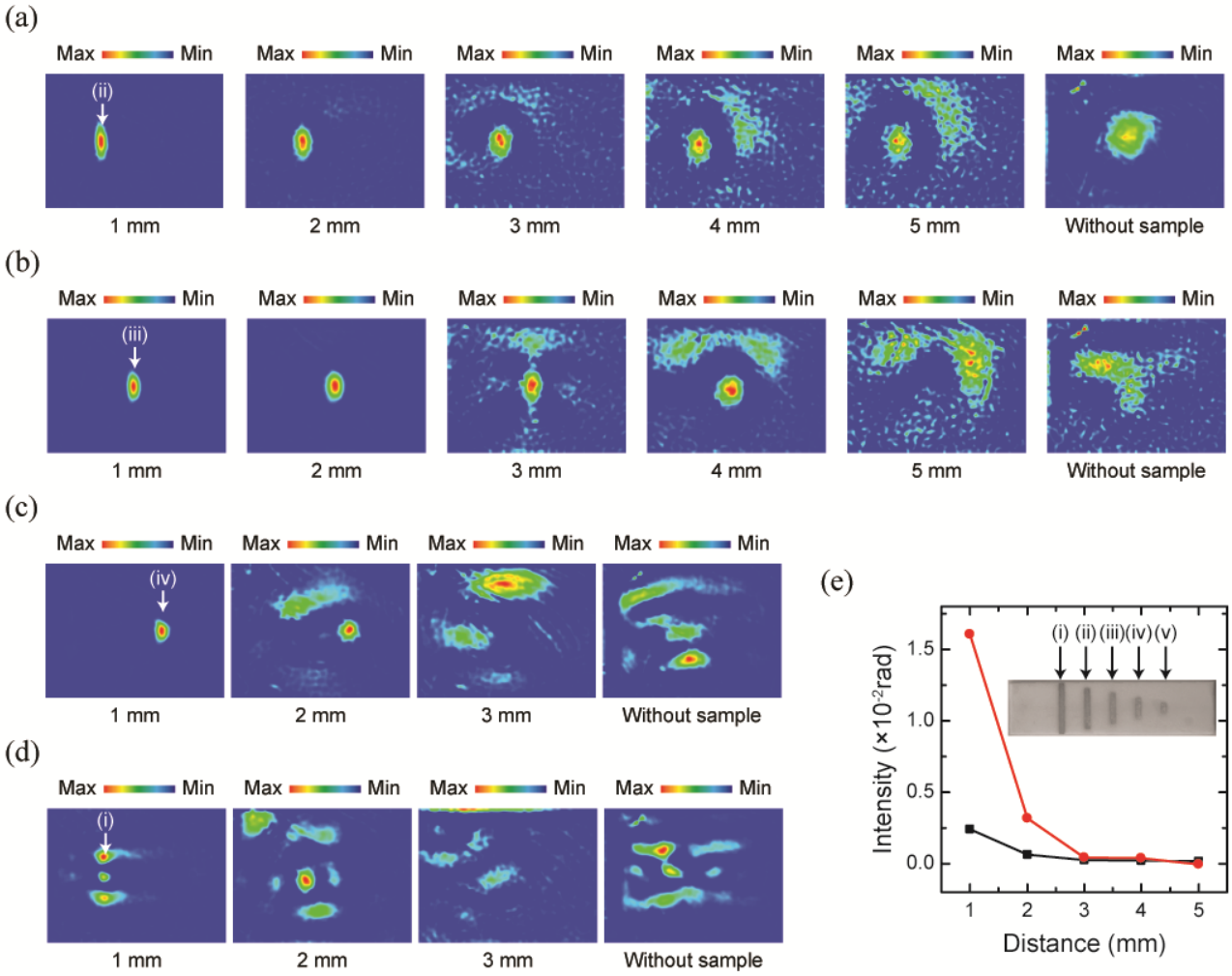


**FIGURE 3.** (a-d) Magnetic microwave near field distribution images of conductive lines measured by TEOIM with different thickness of the optical barrier, where input microwave frequencies for (a-d) are 6.0 GHz, 7.5 GHz, 10.5 GHz, and 15.5 GHz, respectively. In addition, magnetic microwave near field distributions measured without conductive lines are presented. We normalized each image with respect to its maximum intensity to show the structure of the magnetic microwave near field distribution because the intensity was decreased rapidly as the thickness of the optical barrier was increased. The width and height of images were 40 mm and 30mm, respectively. (e) Local intensity changes of measured magnetic microwave near field distributions around conductive lines (ii) (black) and (iii) (red), where the microwave frequencies for (ii) and (iii) were 6.0 GHz and 7.5 GHz, respectively.

TEOIM for the embedded object detection, we patterned conductive lines having different lengths with a width of 1 mm on an alumina substrate (40 mm by 10 mm by 1 mm): (i) 10 mm; (ii) 8 mm; (iii) 6 mm; (iv) 4mm; (v) 2 mm. The patterned sample was attached to a bare and optically opaque alumina substrate (60 mm by 60 mm by 1 mm) so that the patterns were optically invisible. Therefore, the distance between the ITO coated glass and conductive pattern was 2 mm (1 mm air gap and 1 mm alumina barrier).

At first, we will focus on the measurement results for the irradiation microwave frequency less than 10.5 GHz. When the irradiation microwave frequency was lower than 10.5 GHz, the measurement results showed that strong H-MWNF distributions appeared on conductive lines (ii), (iii), and (iv) at 6.0 GHz, 7.5 GHz, and 10.5 GHz respectively. These results indicate that below 10.5 GHz, a shorter conductive line is strongly excited at a higher microwave frequency. In addition, two H-MWNF distributions appeared at the same time when the microwave frequency was 6.5 GHz and 9.0 GHz. By considering that these frequencies are located between frequencies showing a single H-MWNF distribution, appearance of two heat source distributions can be understood as that at an intermediate microwave frequency, two conductive lines that were excited at lower and higher microwave frequencies could be excited at the same time.

The appearance of a single H-MWNF indicates that the excitation of the conductive line shows a resonant characteristic for the irradiated microwave frequency. This resonant behavior was clearly observed from changes of local H-MWNF intensities on conductive lines for the irradiated microwave frequency as appeared in figure 2(c). From measurement results, one can see that the H-MWNF intensities

on conductive lines (iii) and (iv) change like a Lorentzian line shape function, where one can assign peak frequencies of (iii) and (iv) to 7.5 GHz and 10.5 GHz, respectively. These results indicate that the conductive lines behave like an open ended strip-line resonator as discussed in the measurement principle. While H-MWNF intensities on conductive lines (i) and (ii) didn't show a clear Lorentzian line shape at high frequency (>10.5 GHz), they showed a rapid increase and decrease in narrow frequency regions. This result implies that the resonant behavior also appears at the high frequency region. In addition, the intensity on the conductive line (ii) increased as the microwave frequency approached to 6 GHz as shown in the inset of figure 2(c). Because of the bandwidth limit of the microwave amplifier (6∼16 GHz), we couldn't test the microwave frequency region lower than 6 GHz. However, one can expect that the conductive line (ii) will be excited at a lower frequency because the resonance frequency of the open ended strip-line resonator increases as the length decreases. This description is also consistent with the results that the H-MWNF distribution on the conductive line (i) did not appear in the frequency region of 6.0 GHz ∼ 10.5 GHz.

In the frequency region higher than 10.5 GHz, the H-MWNF distribution showed a complicated structure compared to that of low frequency. For instance, the conductive line (ii) showed two H-MWNF distributions at both ends of it, and conductive line (i) showed three H-MWNF distributions at the center and at both ends of it. These H-MWNF distributions are typical structures of a higher order resonance mode of the open ended strip-line resonator, and indicate that a higher order resonance mode appears in the conductive lines at a high frequency region. In addition, a weak but distinguishable H-MWNF appeared along the boundary of the patterned alumina substrate (indicated by a dashed rectangle). This H-MWNF distribution suggests that the present method can also detect a subsurface discontinuity of a dielectric property of a dielectric medium. Although the detection of a discontinuity of the dielectric property will be important for inspection technology on dielectric materials, it is beyond the scope of the present study.

In addition, because the length of the conductive line (v) is shorter than other conductive lines, one can expect that H-MWNF distribution of the conductive line (v) will appear at the high frequency region. However, while conductive lines (i), (ii) and (iv) showed H-MWNF distributions, there was no significant H-MWNF distribution on the conductive line (v) at the high frequency region. This result indicates the amplitude of the H-MWNF generated by the conductive line (v) is not enough to show the heat source distribution. This can be understood since the length of the conductive line (v) is shorter than the others so that the microwave magnetic near field is concentrated in a relatively narrower region than that of other conductive lines. In this case, the amplitude of the near field will decrease more rapidly than other conductive lines. In addition, the amplitude of the near field decreases spatially more rapidly as the microwave frequency increases.

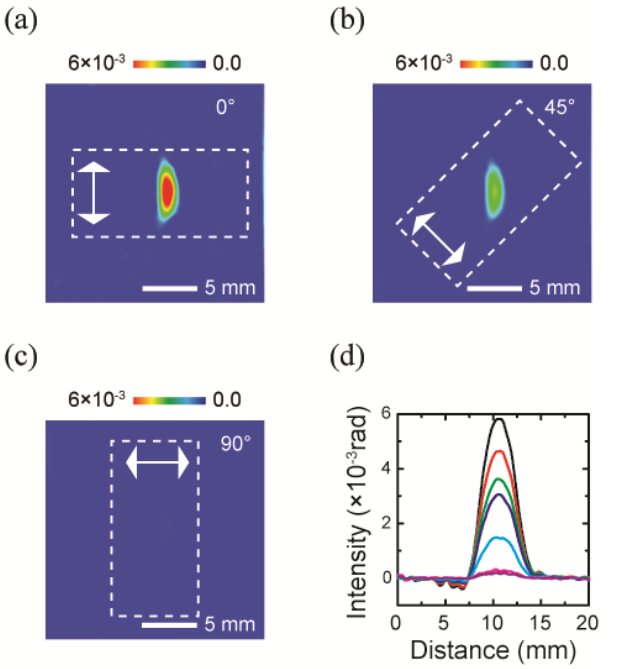


**FIGURE 4.** (a-c) Magnetic microwave near field distribution images of a conductive line (ii) measured by TEOIM with different waveguide orientations. The waveguide orientations are indicated by white dashed rectangles. The input microwave frequency was 7.5 GHz. We indicated white solid lines in images corresponding to 5mm length. (d) Line profiles of magnetic microwave near field distributions around the conductive line for different waveguide orientations: 0° (black); 15° (red); 30° (green); 45° (blue); 60° (cyan); 75° (magenta); 90° (violet).

To verify this explanation, we investigated changes of H-MWNF distributions of conductive lines by increasing the thickness of the dielectric barriers. Figure 3 shows measured H-MWNF distributions of embedded conductive lines with different thicknesses of dielectric barrier from 1 mm to 5 mm. In addition, we measured the H-MWNF distribution of a bare alumina substrate to clearly the contribution of conductive lines to the variation of the H-MWNF distribution. This is because that the H-MWNF distribution of the waveguide changes as a function of input microwave frequency and the distance between the waveguide and the OI as shown in the measurement results. By comparing the H-MWNF distributions measured with and without sample as shown in (a-d), one can see that the H-MWNF distribution of conductive lines (i) (ii), (iii), and (iv) disappear when the thickness of the barrier exceeds 1 mm, 5 mm, 4 mm, and 2 mm, respectively. These results are consistent since as the conductive line became shorter and excited by a higher microwave frequency, its H-MWNF intensity decreased more rapidly. In addition, from (e), one can see that the local H-MWNF intensity of the conductive line (iii) decreases more rapidly than that of the conductive line (ii). This result is consistent since the local H-MWNF intensity will be decreased rapidly as the length of the conductive line decreases and excitation frequency increases. In addition, although a distinguishable H-MWNF distribution of a conductive line disappeared as the thickness of the barrier increased, H-MWNF distributions measured

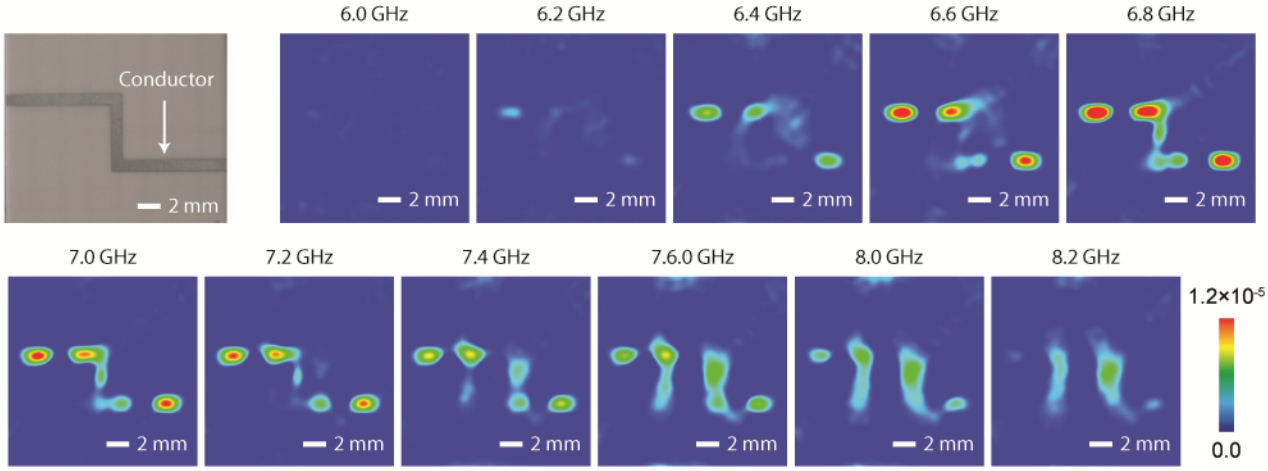


**FIGURE 5.** Optical image of the conductive line and its magnetic microwave near field distribution images measured by TEOIM for different microwave frequencies from 6.0 GHz to 8.2 GHz. The width and height of images are 40 mm and 30 mm, respectively. We indicated white solid lines in images corresponding to 2 mm length.

with and without sample are quite different from each other. These results imply that although it is difficult to directly predict an exact structure of a deeply embedded object from the H-MWNF distributions, one can find its existence from a change of the H-MWNF distribution.

The excitation efficiency of a strip-line resonator is dependent on the polarization direction of the excitation microwave. Therefore, the intensity of the H-MWNF distribution of the conductive line will be sensitive to the relative direction of the microwave polarization and the conductive line. To verify this, we visualized H-MWNF distribution with different orientation of the waveguide for the fixed conductive line (ii). Figure 4 (a-c) show representative H-MWNF distributions measured with different orientations of the horn antenna (indicated by dashed rectangles) of 0°, 45°, and 90°, and (d) show intensity line profiles of H-MWNF distributions measured with different orientations of the horn antenna. From the results, one can see that the H-MWNF intensity decreases when the long directions of the horn antenna and conductive line become parallel to each other. Because the horn antenna was connected with a TE-mode wave guide, the electric and magnetic field directions of the irradiated microwave were parallel and perpendicular to the short direction of the horn antenna (indicated by bi-directional arrows), respectively. Therefore, these results indicate that the detection efficiency of the conductive lines is maximized when the microwave electric (magnetic) field direction is parallel (perpendicular) to the length direction of the conductive line. Therefore, for a practical case where conductive lines with arbitrary orientations are distributed in a dielectric medium, one needs to measure the H-MWNF distributions with various polarization directions of the irradiated microwave. We note that this can be done just by changing the polarization direction of the microwave by rotating the horn antenna without modifying the TEOIM system.

Finally, we tested detection of a structure consisting of a long continuous conductive line as shown in Figure 5. This is a good example for applications for the non-contact and non-destructive characterization of an electric or monolithic microwave integrated circuit embedded in a dielectric medium. From the measurement results, where the conductive line was covered by an alumina plate (1 mm thickness), one can see that H-MWNF distributions appear along the conductive line in the microwave frequency range of 6.4∼7.4 GHz. This result clearly indicates that one can find a structure of a conductive circuit underlying an optically opaque dielectric material in non-contact and non-destructive way.

## V. CONCLUSION

In conclusion, we presented the subsurface imaging of a conductive object embedded in an optically opaque dielectric medium by using TEOIM system. By visualizing H-MWNF of the conductive object emerging from the dielectric medium, we showed that one can detect embedded conductive object from the H-MWNF distribution. We presented the detection performance of present method for the embedded conductive object for various lengths, orientations, and subsurface depth. From the present results, one can expect that the present method can be an attractive candidate for a practical inspection system for the subsurface detection of a conductive object embedded in a dielectric medium.

## REFERENCES

[1] S. Kharkovsky and R. Zoughi, "Microwave and millimeter wave nondestructive testing and evaluation-Overview and recent advances," *IEEE Instrum. Meas. Mag.*, vol. 10, no. 2, pp. 26–38, Apr. 2007.

[2] L. You, J.-J. Ahn, Y. S. Obeng, and J. J. Kopanskiet, "Subsurface imaging of metal lines embedded in a dielectric with a scanning microwave microscope," *J. Phys. D, Appl. Phys.*, vol. 49, Dec. 2016, Art. no. 045502.

[3] G. Gramse *et al.*, "Quantitative sub-surface and non-contact imaging using scanning microwave microscopy," *Nanotechnology*, vol. 26, no. 13, 2015, Art. no. 135701.
[4] G. Gramse *et al.*, "Nondestructive imaging of atomically thin nanostructures buried in silicon," *Sci. Adv.*, vol. 3, Jun. 2017, Art. no. e1602586.
[5] C. Plassard *et al.*, "Detection of defects buried in metallic samples by scanning microwave microscopy," *Phys. Rev. B, Condens. Matter*, vol. 83, Mar. 2011, Art. no. 121409.
[6] N. K. Nikolova, "Microwave imaging for breast cancer," *IEEE Microw. Mag.*, vol. 12, no. 7, pp. 78–94, Dec. 2011.
[7] Y. J. Kim, L. Jofre, F. D. Flaviis, and M. Q. Feng, "Microwave reflection tomographic array for damage detection of civil structures," *IEEE Trans. Antennas Propag.*, vol. 51, no. 11, pp. 3022–3032, Nov. 2003.
[8] G. Charvat, A. Temme, M. Feigin, and R. Raskar, "Time-of-flight microwave camera," *Sci. Rep.*, vol. 5, p. 14709, Oct. 2015.
[9] L. Wang, L. Li, Y. Li, H. C. Zhang, and T. J. Cui, "Single-shot and single-sensor high/super-resolution microwave imaging based on metasurface," *Sci. Rep.*, vol. 6, p. 26959, Jun. 2016.
[10] Y. Xie, X. Fan, Y. Chen, J. D. Wilson, R. N. Simons, and J. Q. Xiao, "A subwavelength resolution microwave/6.3 GHz camera based on a metamaterial absorber," *Sci. Rep.*, vol. 7, p. 40490, Jan. 2017.
[11] K. Sasagawa, A. Kanno, T. Kawanishi, and M. Tsuchiya, "Live electrooptic imaging system based on ultraparallel photonic heterodyne for microwave near-fields," *IEEE Trans. Microw. Theory Techn.*, vol. 55, no. 12, pp. 2782–2791, Dec. 2007.
[12] M. Tsuchiya, S. Fukui, and M. Yorinaga, "Microscopic live electrooptic imaging," *Sci. Rep.*, vol. 7, p. 7917, Aug. 2017.
[13] H. Lee, S. Arakelyan, B. Friedman, and K. Lee, "Temperature and microwave near field imaging by thermo-elastic optical indicator microscopy," *Sci. Rep.*, vol. 6, p. 39696, Dec. 2016.
[14] N. Yoshikawa, "Fundamentals and applications of microwave heating of metals," *J. Microw. Power Electromagn. Energy*, vol. 44, no. 1, pp. 4–13, 2010.
[15] H. Bosman, Y. Y. Lau, and R. M. Gilgenbach, "Microwave absorption on a thin film," *Appl. Phys. Lett.*, vol. 82, p. 1353, Mar. 2003.
[16] S. Arakelyana, H. Lee, Y. Jeong, A. Babajanyan, B. Friedman, and K. Lee, "Direct imaging of the SSD and USB memory drives heating by thermo-elastic optical indicator microscopy," *Case Stud. Thermal Eng.*, vol. 10, pp. 407–412, Sep. 2017.
[17] T. Ishibashi *et al.*, "Magneto-optical imaging using polarization modulation method," *J. Appl. Phys.*, vol. 100, Nov. 2006, Art. no. 093903.

**HANJU LEE** received the B.A. degree in physics, the M.S. degree, and the Ph.D. degree in physics from Sogang University, Seoul, South Korea, in 2006, 2008, and 2016, respectively, where he is currently a Researcher. His current research interests include magneto-optics, organic semiconductors, spintronics, microwave imaging, and microwave memristive devices.

**ZHIRAYR BAGHDASARYAN** was born in Areni, Armenia. He received the M.S. degree in radiophysics from Yerevan State University, Yerevan, Armenia, in 2017. He is currently a Researcher with Sogang University, Seoul, South Korea. His current research interests include visualization techniques, and optical and microwave sensors.

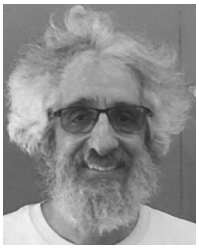

**BARRY FRIEDMAN** received the B.A. degree in physics from Rice University, Houston, TX, USA, in 1978, and the Ph.D. degree in physics from the University of Illinois at Urbana-Champaign, Champaign, IL, USA, in 1985, where his thesis advisor was Y. Oono. He is currently a Professor of physics with Sam Houston State University, Huntsville, TX, USA. He has been a Visiting Scientist with the Electro Technical Lab, Tsukuba, Japan, and Institute of Solid State Physics, Tokyo, Japan. His current research interests include theoretical and computational solid state, and chemical physics.

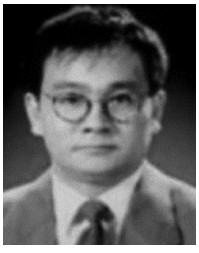

**KIEJIN LEE** received the B.A. and Ph.D. degrees in physics from Sogang University, Seoul, South Korea, in 1986 and 1989, respectively, where he is currently a Professor with the Department of Physics and Basic Science Institute for Cell Damage Control. He has authored over 100 journal publications. His current research interests include the design and characterization of microwave nearfield microscopy and biosensors.